ENGINE AIRFRAME INTEGRATION STUDIES USING THE CFD++ CODE

Francisco José de Souza
Universidade Federal de Uberlândia
Av. João Naves de Ávila, 2160
Uberlândia – MG – Brazil
e-mail: fjsouza@mecanica.ufu.br

Aristeu da Silveira Neto
Universidade Federal de Uberlândia
Av. João Naves de Ávila, 2160
Uberlândia – MG – Brazil
e-mail: aristeus@mecanica.ufu.br

Sigeo Kitatani Junior
Universidade Federal de Uberlândia
Av. João Naves de Ávila, 2160
Uberlândia – MG – Brazil
e-mail: sigeojr@yahoo.com

João Luiz F. Azevedo
Instituto de Aeronáutica e Espaço
CTA/IAE/ASE - N
12228-904 – São José dos Campos – SP – Brazil
e-mail: azevedo@iae.cta.br

Antonio Batista de Jesus
Embraer – Empresa Brasileira de Aeronáutica
Av. Brigadeiro Faria Lima, 2170
12227-901 - São José dos Campos – SP – Brazil
e-mail: antonio.jesus@embraer.com.br

Guilherme Lara de Oliveira
Embraer – Empresa Brasileira de Aeronáutica
Av. Brigadeiro Faria Lima, 2170
12227-901 - São José dos Campos – SP – Brazil
e-mail: guilherme.oliveira@embraer.com.br

Abstract. *It is well known in the aricraft industry that the integration of engines into the aircraft involves many different aspects. These aspects can be investigated by means of wind tunnel experiments or numerical simulation. In this paper, a computational engine airframe integration study is reported. The aircraft geometry investigated is the DLR-F6 configuration. Since the interest has been mainly in the cruise condition, only the half-span model is considered. The hexahedral grids used were generated with the ICEM code. In order to evaluate installation effects, the model is first simulated without the engines (nacelle and pylon). The drag, lift and pressure coefficients are then evaluated. The nacelle and pylon are added to the model and the aerodynamic coefficients computed for this configuration. The pressure coefficients on the wing display important differences when the engine is added. The computed results agree well with the experimental data. Based on the visualization of the flowfield, the physical phenomena that take place in engine/airframe integration are discussed.*

Keywords*: engine/airframe integration, DLR-F6, hexahedral mesh.*

1. Introduction

According to Harris (1992), engine airframe integration is defined as 'that process which is used whenever the performance of the integrated engine airframe, when operated in a designed combination, is significantly different from the sum of the individual engine and airframe performances, that is, for given values of flight Mach number, angle of attack and power setting'. Nicholson's argument was that 'the aircraft cannot be conceived first and the propulsive units considered afterwards' (Nicholson, 1957). To a very large degree, it can be argued that the engine airframe integration process is at the heart of the overall aircraft design process. The focus in design of an aircraft must not rest too long on the individual components or the integration process will be entered too late and then the production can get very costly in time, manpower and in terms of lack of performance achievement.

Computational Fluid Dynamics (CFD) has been extensively used in the aircraft industry to evaluate aerodynamic performance during the conceptual and preliminary design stages. With the recent advances in CFD and computer capabilities it is now possible to simulate complete airplane configurations in a short enough period of time and to have a significant impact on the design cycle. It is generally agreed that CFD is a valuable tool for evaluating the rate of change in the aerodynamic characteristics (such as drag or lift) due to design alterations. Nevertheless, there is still significant uncertainty about the accuracy of CFD for predicting the absolute value of the aerodynamic characteristics, particularly the drag coefficient. As a result of this lack of confidence, the current state of the art is to use CFD as a tool for screening a large number of potential designs. The best candidates are then selected for further testing in a wind tunnel where the actual values of the aerodynamic characteristics are measured and used for all the performance calculations.

In this study, the test case chosen is the DLR-F6 configuration without (WB – wing-body) and with underwing-mounted engines (WBNP – wing-body-nacelle-pylon). This is a public domain geometry and there is a large body of high-quality experimental data available. Drag and lift coefficients were computed and compared to the experimental data at the design point for each configuration (WB and WBNP). Also, the pressure coefficients on different spanwise locations were compared with experiments. In general, the agreement was found to be satisfactory. It was observed that the inclusion of the nacelle/pylon caused supersonic/transonic regions to build up on the lower wing surface. Such an effect is virtually non-existent in the clean configuration (WB).

2. The test case

Figure 1 illustrates the DLR-F6 model (Brodersen and Stürmer, 2001) with engines mounted under the wings (WBNP), which was one of the configurations simulated in this work. This configuration is relatively complex and represents a typical twin-engine wide body aircraft.

A picture of the wind tunnel in which the experiments were run (2nd DPW, 2003) is displayed in Fig. 2.

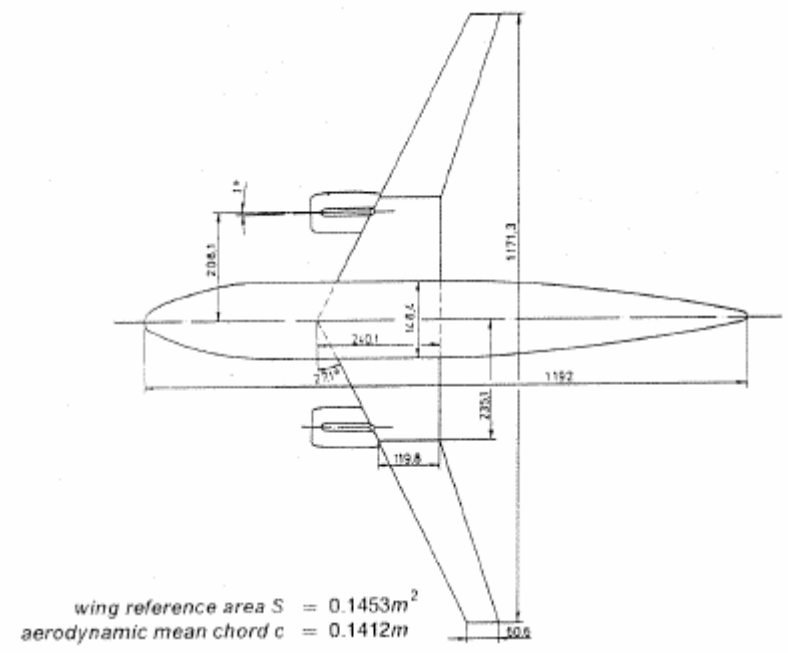

Figure 1 – DLR-F6 geometry with underwing–mounted engine-pylons (quotes in mm) (WBNP) (Brodersen and Stürmer, 2001).

The mean aerodynamic chord of the DLR-F6 is 0.1412 m, and its half-model reference area is 0.0727 m^2. The nacelle centerline is defined by the following two points:

Point 1: x=-8.73756 mm, y=-205.39937 mm, z=-28.54676 mm.

Point 2: x= 203.95542 mm, y= -209.07073 mm, z= -35.98394 mm.

The design point of the DLR-F6 corresponds to Mach number $M_\infty = 0.75$ and Reynolds number $Re = 3 \times 10^6$. Also, the experiments were run at the temperature of 305 K. The design lift coefficient under these conditions is 0.5, which corresponds to the experimental angle of attack of 1.0^o for the configuration with pods on (WBNP) and 0.52^o for the clean configuration (WB). The Reynolds number is based on the aerodynamic mean chord of the model.

The engines in this model were represented by through-flow nacelles. The experimental test campaigns were performed between 1993 and 1996 in the ONERA S2MA pressurized wind tunnel. The model was sting-mounted in the

transonic test section and the Mach number was varied between 0.6 and 0.8, while the Reynolds number was held constant at Re = 3 x 10^6. For the design Mach number, the drag polar was measured for the DLR-F6 configuration with and without the engines at angles of attack from -5 ^{o} to +2 ^{o}.

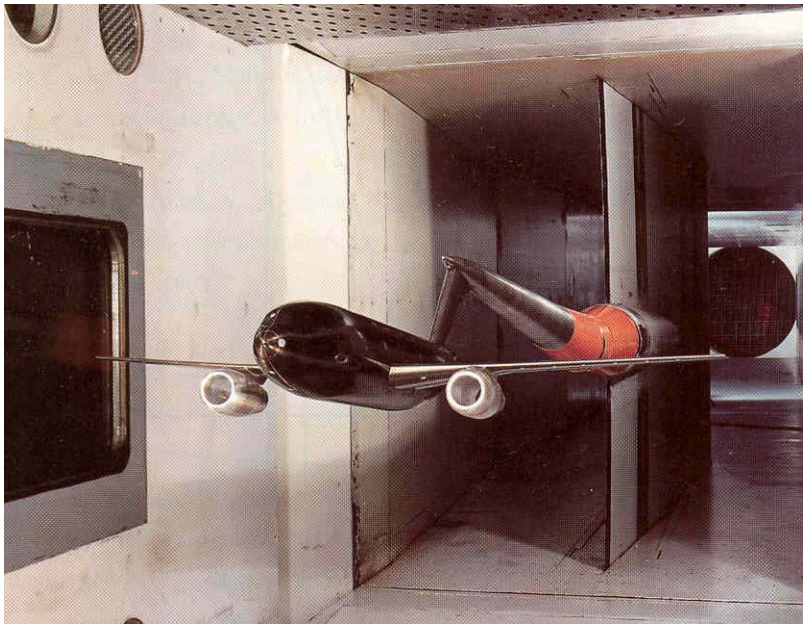

Figure 2 – Wind tunnel model reference geometry of DLR-F6 (WBNP) (2nd DPW, 2003).

3. Setup of the simulations

Since the main interest of this investigation is in the cruise condition, only half-span models were considered. The grids contained nearly 2.6 and 5.8 million hexahedral elements for the clean configuration (WB) and the configuration with pylon/nacelle (WBNP), respectively. Both grids were created with the mesh generator ICEM 5.0. In order to compute the flow around both DLR-F6 configurations (WB and WBNP), the commercial code CFD++ was used. Freestream boundary conditions were set as in the experiments (T=305 K, M_∞ = 0.75, Re = 3 x 10^6), with the turbulence intensity equal to 0.1 % and the turbulence viscosity/molecular viscosity ratio equal to 1. According to the information at the website of the 2nd Drag Prediction Workshop (2003), the angles of attack at the design point are 0.52 ^{o} for the clean configuration (WB) and 1.0 ^{o} for the configuration with engines (WBNP). The conditions above were also used as initial conditions. On all the solid surfaces, the advanced wall functions available in CFD++ were used. The turbulence model chosen was the realizable κ-ε model.

The simulations were run on a Linux cluster and used 10 CPU's.

4. Results

Table 1 compares the drag and lift coefficients computed for both configurations with experimental values. The numerical coefficients are seen to be below the experimental ones, particularly for the configuration with pods on (WBNP). This might be due to a number of reasons, such as insufficient mesh refinement at the nacelle inlet, boundary conditions, or even the uncertainty of the numerical itself. Nevertheless, it is important to bear in mind that these results are not poorer than the ones provided by other simulations, which normally report errors in the prediction of the coefficients in the same order (2nd DPW, 2003). The pressure coefficient at various spanwise locations on the wing for the clean configuration is shown in Fig. 3. In general, the agreement is very good compared to the experiments.

Table 1 – Drag and lift coefficients for the DLR F6 WB and DLR F6 WBNP at the design point.

	C_d	C_l
Experimental WB	0.0295	0.5000
Simulated WB	0.0284	0.5026
Experimental WBNP	0.0338	0.5000
Simulated WBNP	0.0378	0.5310

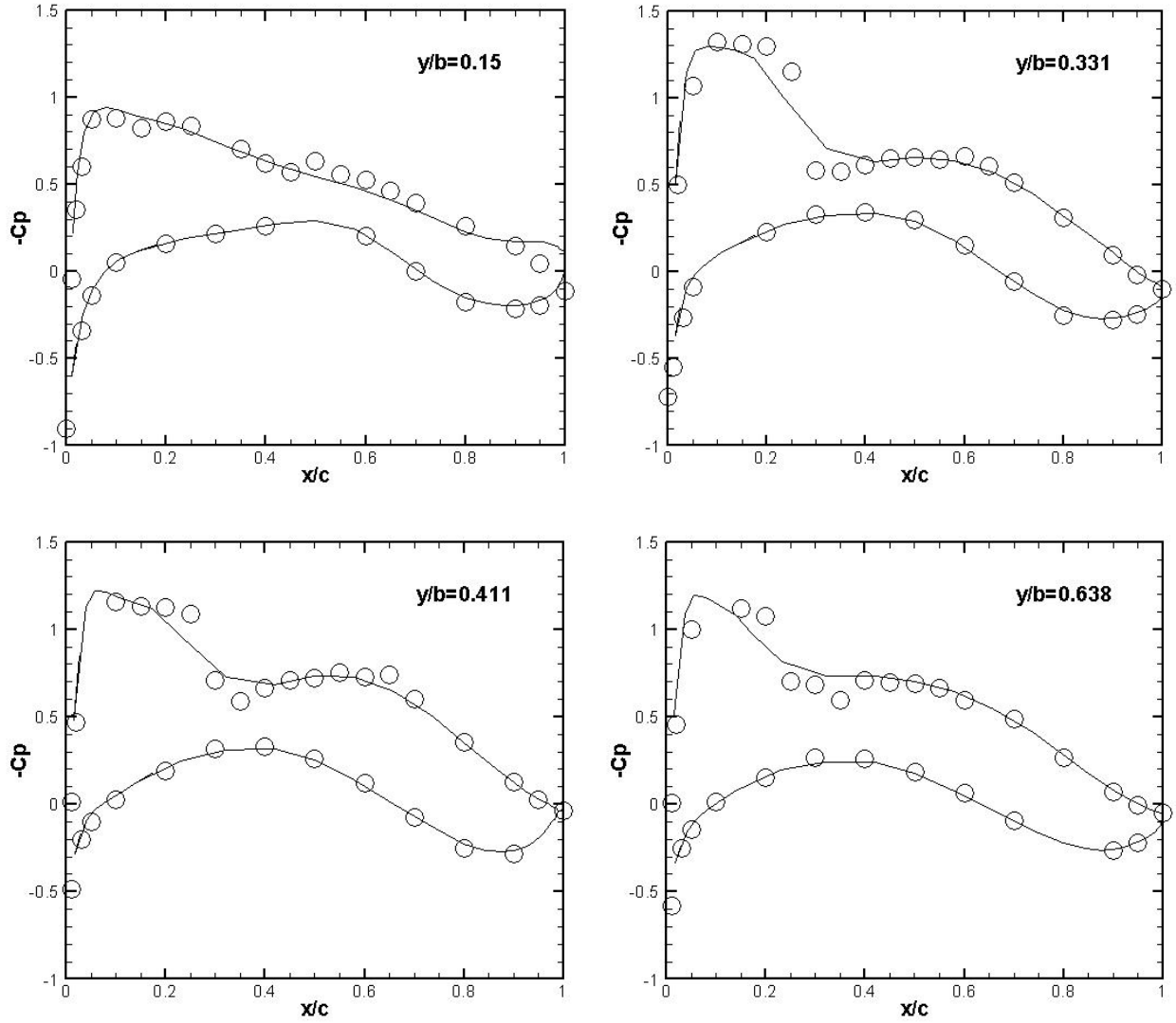

Figure 3 – Measured and computed pressure coefficient at 15 %, 33.1 %, 41.1 % and 63.8 % span for the clean DLR F6 (WB). Circles represent the experimental data, the line represents the computed results.

The pressure coefficient at the same spanwise locations for the DLR-F6 model with engines is shown in Fig. 4. It can be seen that the quality of the predictions is not as good as that for the clean model, particularly for $x/c < 0.4$ and $y/b > 0.4$. In these regions, the pressure predicted on the upper surface is higher than the experimental one and this possibly contributed to the larger error in the lift coefficient prediction for the DLR-F6 with engines (WBNP), shown in Table 1. This might be attributed to a number of reasons, which shall be investigated. At 33.1 % span, it can be seen that the experimental pressure for the DLR-F6 WBNP nearly equal between 20 % and 30 % of the chord, clearly indicating the lift loss brought about by the pylon/nacelle installation. Even though the simulation slightly overpredicts the pressure on the upper wing and underpredicts it on the lower surface, this conclusion would have possible based only on the computed pressure coefficients.

Important conclusions can be drawn based on the visualization of the simulated flow. A comparison between the simulated flow field and experimental oil-flow visualization (2nd DPW, 2003) is presented in Fig. 5. Fig. 5(a) clearly shows evidence of reverse flow at the junction wing-fuselage and close to the kink on the upper wing. The simulation suggested the existence of these recirculation regions, as can be seen in Fig. 5(b), which displays the isosurfaces of negative streamwise velocity U=-1.0 m/s. These reverse flow regions were also observed in the simulated clean configuration and therefore are not due to pylon/nacelle installation effects, as shown in Fig. 5(c).

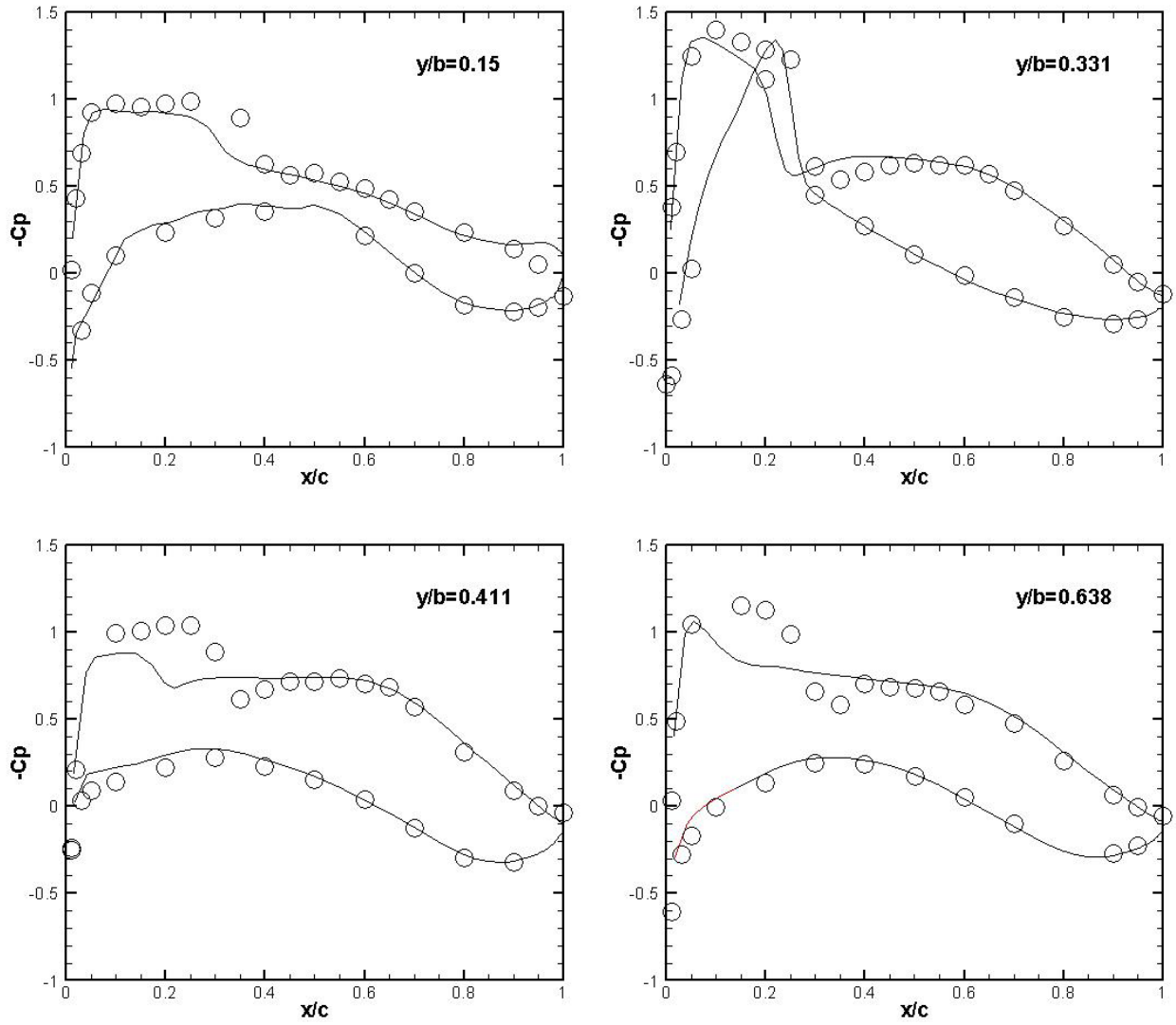

Figure 4 – Measured and computed pressure coefficient at 15 %, 33.1 %, 41.1 % and 63.8 % span for the clean DLR F6 (WBNP). Circles represent the experimental data, the line represents the computed results.

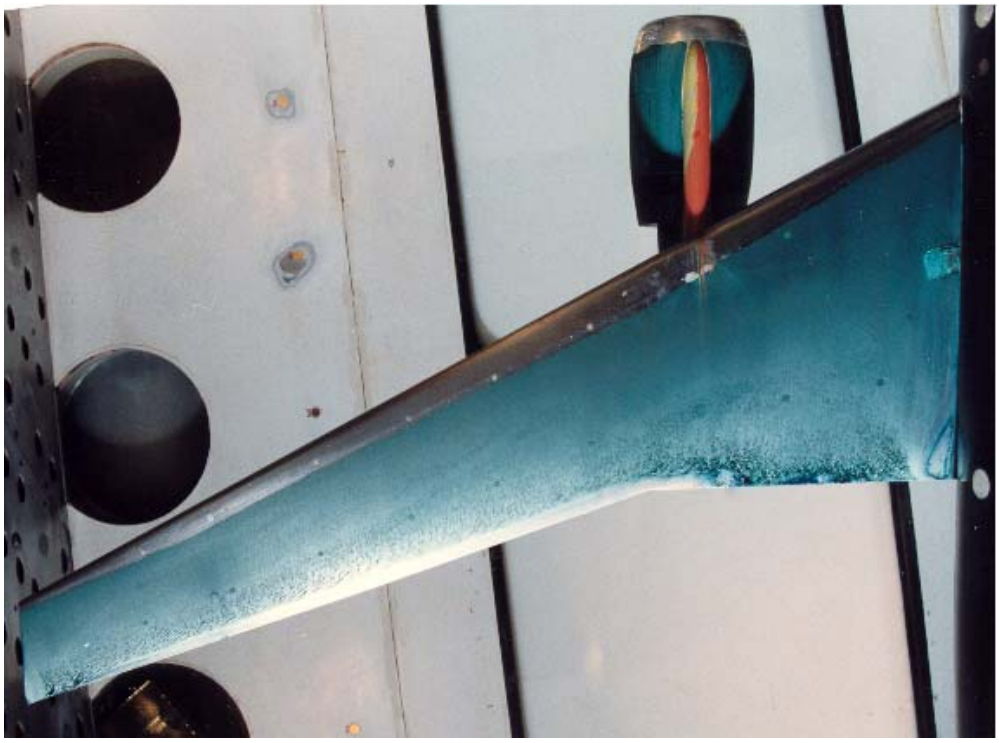

5(a)

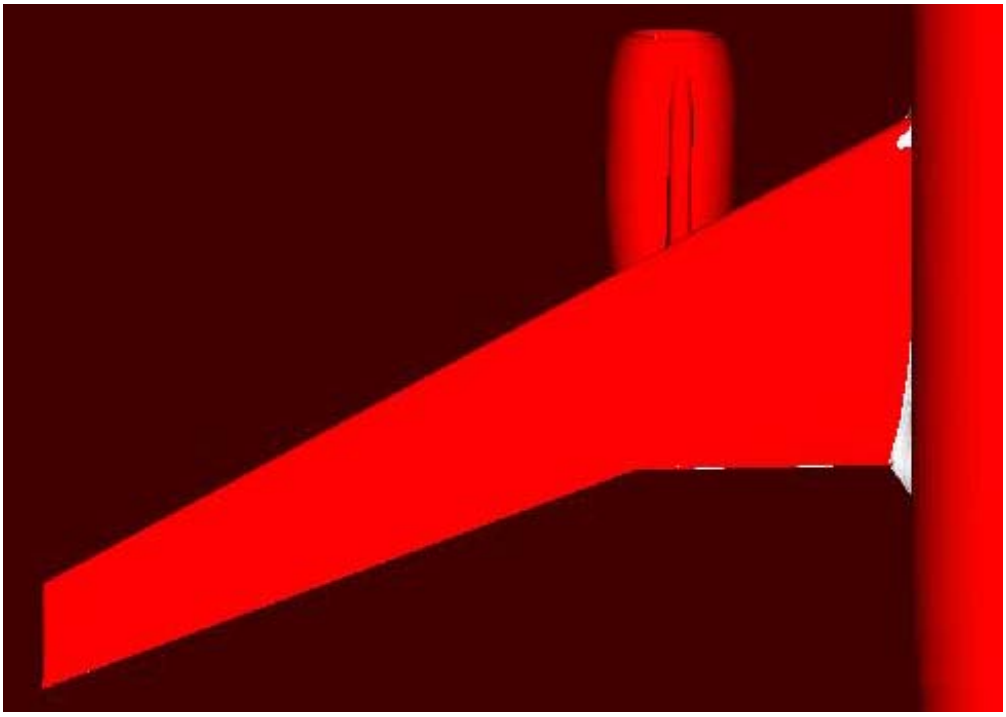

5 (b)

Figure 5 – Experimental oil-flow visualization (5a), isosurfaces of negative streamwise velocity U = -1.0 m/s in the DLR-F6 WBNP (5b) and DLR-F6 WB (5c), indicating reverse flow.

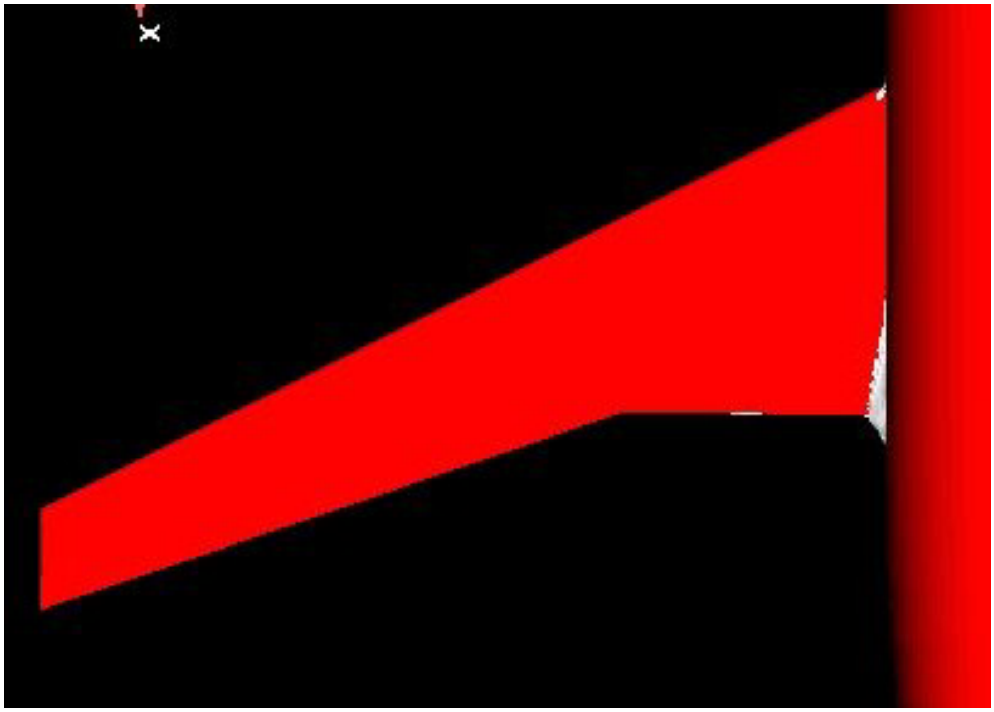

5 (c)

Figure 5 – Experimental oil-flow visualization (5a), isosurfaces of negative streamwise velocity U = -1.0 m/s in the DLR-F6 WBNP (5b) and DLR-F6 WB (5c), indicating reverse flow (cont.).

An installation effect on the lower wing can be observed in Fig. 6. Due to the "virtual channel" between the pylon, the nacelle and the lower wing surface, the flow is accelerated and its pressure drops under the wing, as shown in Fig. 6. This effect, in turn, causes a reduction in the aircraft lift, as commented by Rudnik et al (2002). Also shown in Fig. 6 is the isosurface of Mach number M=1.2, which reveals that transonic/supersonic regions in the vicinity of the pylon may also result from the pod installation. These regions are virtually inexistent in the clean model.

5. Conclusions

Accurate results for the drag, lift and pressure coefficients for the public geometry DLR-F6 have been computed by using the commercial code CFD++. Important engine airframe integration effects have been investigated numerically and by means of the flow field visualization.

6. Acknowledgements

The authors wish to thank Embraer for the support provided for this work.
The authors also acknowledge the support of Fundação de Amparo à Pesquisa do Estado de São Paulo, FAPESP, through the Research Grant No. 2000/13768-4.

7. References

Brodersen, O. and Stürmer, A., 2001, Drag Prediction of Engine-Airframe Interference Effects using Unstructured Navier-Stokes Calculations, AIAA-2414.

Harris, A. E., 1992, Test Techniques for Engine/Airframe Integration, AGARD 69th Fluid Dynamics Panel Meeting and Symposium on Aerodynamic Engine/Airframe for High Performance Aircraft and Missiles.

Nicholson, L. F., 1957, Engine-airframe integration, RAeS Lecture, April 1957 (published in RAeS Journal Vol 61 Nov. 1957).

Rudnik, R., Rossow, C. -C. and v. Geyr, H. F., 2002, "Numerical Simulation of Engine/Airframe for High Bypass Engines", Aerospace Science and Technology 6, pp. 31-42.

2nd DPW, 2003, 2nd Drag Prediction Workshop, http://ad-www.larc.nasa.gov/tsab/cfdlarc/aiaa-dpw/.

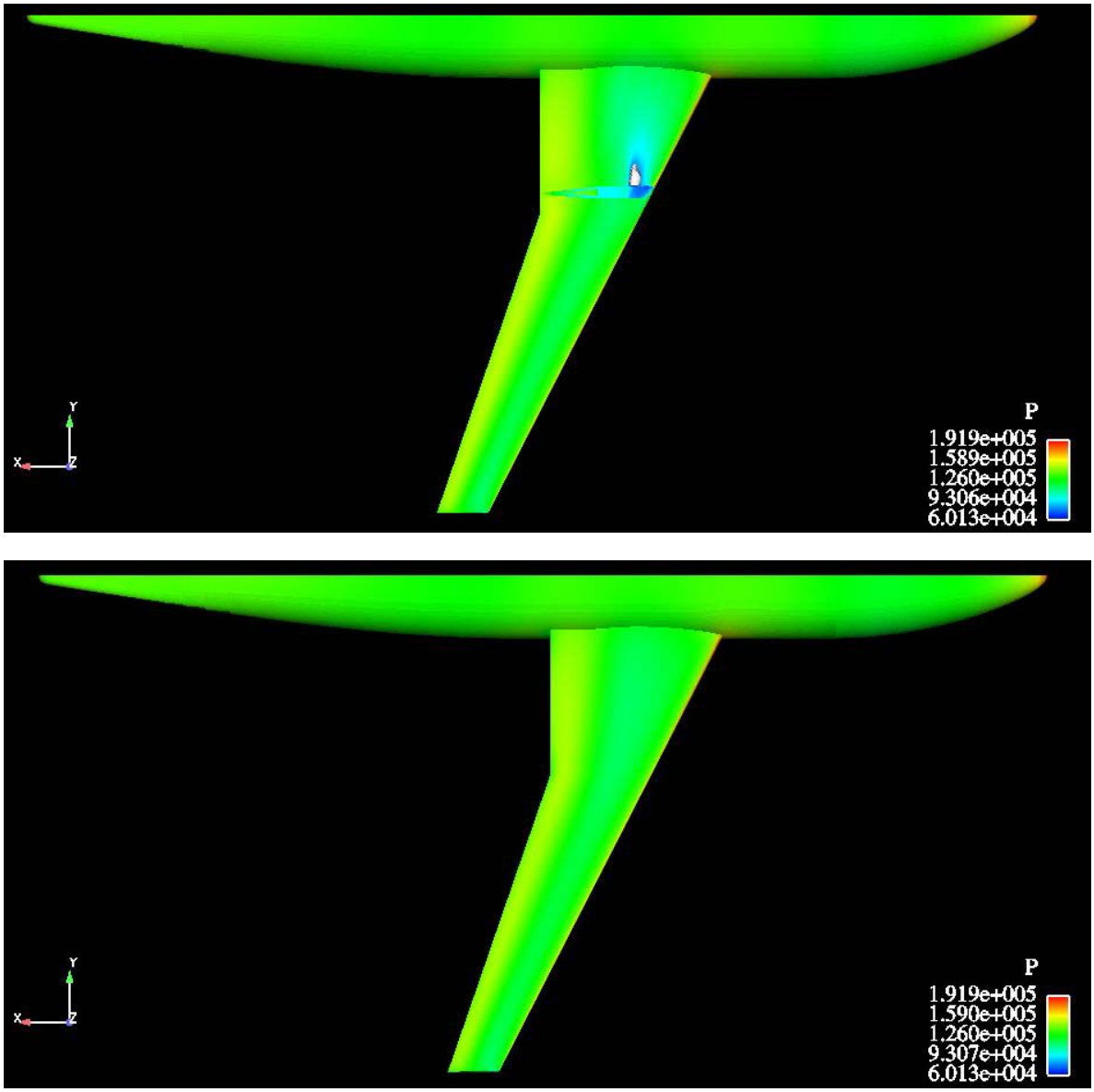

Figure 6 – Pressure distributions and isosurfaces of Mach number 1.2 on the lower wing of the DLR-F6 WBNP and the DLR-F6 WB, showing the confinement effect due to the installation of the pylon/nacelle and the existence of supersonic regions in the vicinity of the pylon.

8. Responsibility notice

The authors are the only responsible for the printed material included in this paper.